Available online at www.sciencedirect.com
ScienceDirect
Trans. Nonferrous Met. Soc. China 24(2014) 22−27
Transactions of Nonferrous Metals Society of China
www.tnmsc.cn

Abnormal precipitation behavior in T6 melt-spun AlMgCu ribbon

Zhong-wei CHEN, Ming-jun TANG, Shi-shun LI, Zong-qiang FENG

State Key Laboratory of Solidification Processing, Northwestern Polytechnical University, Xi'an 710072, China

Received 12 October 2012; accepted 30 January 2013

Abstract: The constituent of precipitations phases of aged melt-spun AlMgCu ribbons was characterized by high-resolution transmission electron microscopy and microhardness test. The cooling rate of as melt-spun ribbon was estimated to be 1.60×10^5 K/s from the empirical relation. The samples were aged at 200 °C for 16 h after solution treatment. Two precipitation phases, i.e. Al_2CuMg and abnormal amorphous SiO_2 were identified in the T6 melt-spun AlMgCu ribbon. The crystal structure and stoichiometric composition of Al_2CuMg phase are in good agreement with the reference results [WANG et al (2007; 2005)]. The combined experiments show that the formation of abnormal amorphous SiO_2 appears to be associated with the higher cooling rate in melt-spinning process and has no significant effect on the peak hardness.

Key words: AlCuMg alloy; melt spinning; precipitation; amorphous

1 Introduction

As important structural materials, AlCuMg alloys are widely used in the aerospace and automotive industry. So far, there is limited report on the precipitation behavior for the Cu-lean alloys [1−4] compared to the Cu-rich alloys [5−9]. RATCHEV et al [10] believed that the age-hardening characteristics of the AlMgCu alloys (Cu-lean) were similar to those in the AlCuMg alloys (Cu-rich) in several respects. Besides a precipitation sequence for these ageing alloys proposed by BAGARYATSKY [11], the observed precipitation sequence for the Si-containing AlCuMg alloys at 200 °C involves SSS + $Mg_2Si\rightarrow\alpha$ + Si-modified GPB zones + $Mg_2Si\rightarrow$ α + S + Mg_2Si [7], where SSS stands for supersaturated solid solution and GPB stands for Guinier-Preston-Bagaryatsky [12]. Here, the S phase, which represents the equilibrium phase Al_2CuMg, has a face-centered orthorhombic structure with the lattice parameters a=0.400 nm, b=0.923 nm, c=0.714 nm, always forms on $\{012\}_{Al}$ habit planes and grows mainly along $\langle100\rangle_{Al}$ directions [5,13,14].

Moreover, the additions of Si and Ag can greatly affect the age hardening characteristic of AlCuMg alloys by modifying the nucleation of precipitates. And an understanding of the underlying mechanisms for this effect is necessary to elucidate rational alloy design principles [15,16]. The addition of Si to these alloys accelerated the interaction of solutes, and fine scale precipitates rich in Mg and Cu and containing traces of Ag and Si, were detected immediately following the rapid hardening reaction [15]. A series of AlCuMg−(Ag)−Si alloys were prepared to investigate the role of Si addition in the formation of precipitation phase, and trace amount of Si was found to quell precipitation, indicating that it was necessary to overcome a critical Mg to Si ratio for nucleation in this alloy system [17]. MUKHOPADHYAY [18] showed that various constituent phases, such as Mg_2Si, Al_2CuMg, and $Al_{12}(Fe{-}Mn)_3Si$, Mn-bearing dispersoids that were formed during homogenization treatment and dissolved a certain proportion of Si, may tie up a significant proportion of Si and markedly reduce the driving force for some precipitation during artificial ageing. Increasing Si content also enhanced the formation of Type I S phase during differential scanning calorimetry (DSC) experiments, and decreased the formation of Type II S phase [19].

The hypothesis of this work is that by applying a rapid solidification process (RSP), melt spinning, it is possible to retain higher quantities of alloying elements

Foundation item: Project (42-QP-009) supported by Research Fund of the State Key Laboratory of Solidification Processing, China; Project (Z2012019) supported by Graduate Starting Seed Fund of Northwestern Polytechnical University, China; Project (B08040) supported by the Program of Introducing Talents of Discipline to Universities ("111" Project), China

Corresponding author: Zhong-wei CHEN; Tel: +86-29-88493450-8001; E-mail: chzw@nwpu.edu.cn

DOI: 10.1016/S1003-6326(14)63023-5

in solid solution and thereby modify the precipitation process. RSP allows a reduction in grain size, extends solid solution ranges, reduces levels of segregation and, in some cases, the formation of metastable crystalline and amorphous phases by cooling metallic melts at cooling rates exceeding 10^4 K/s [20−22]. Furthermore, the decomposition of a supersaturated solid solution in melt-spun alloys is usually accompanied by recrystallization, affecting the aged microstructures and the corresponding properties. Different explanations have been offered to infer the strengthening mechanism for RSP alloys. One argues that phases precipitate prior to recrystallization and impede the movement of dislocations, which then inhibit the recrystallization process. The other explains the favorable effect of recrystallization by the fact that recrystallization greatly refines the grain size and disperses the precipitates, resulting in higher microhardness after ageing [23].

In this study, high-resolution transmission electron microscopy (HRTEM) and conventional transmission electron microscopy (TEM) techniques were used to study the major constituent precipitations on an artificially aged melt-spun AlMgCu ribbon containing 0.22% Si. The phases were determined by selected area electron diffraction (SAED) analyses. The chemical compositions of the precipitations were determined by an energy dispersive spectroscope (EDS) and were compared with the stoichiometric compositions of the compounds. The effect of various precipitates present for the strengthening of the alloys was also discussed.

2 Experimental

The feedstock AlMgCu alloy was produced by direct-chill (DC) casting with a chemical composition given in Table 1, followed by melt-spinning into ribbons on a single copper wheel with a diameter of 28 cm at the rotating speed of 20 m/s. The melt-spun ribbons prepared had a width of about 5 mm and a thickness of 46 μm.

Table 1 Chemical composition of AlMgCu alloy (mass fraction, %)

Cu	Mg	Si	Fe	Mn	Cr
0.50	1.99	0.22	0.19	0.003	0.002
Ni	Zn	Ti	B	Al	
0.004	0.002	0.005	0.001	Balance	

The samples of as melt-spun ribbons were solution heat treated at 550 °C for 20 min, followed by quenching in water, and ageing at 200 °C for 16 h in a temperature-controlled oil bath. The Vickers hardness values of the as melt-spun sample and aged sample were measured in HXP−1000M microhardness tester at the load of 100 g. The microstructure of these alloys was observed on a Tecnai F30 G^2 TEM using the bright field imaging technique, and the precipitation phases were determined by HRTEM, SAED and EDS. TEM samples of 3 mm in diameter were electro-polished in a 70% ethanol and 30% nitric acid solution at −26 °C, by using a twin-jet equipment operated at 30 V.

3 Results

Figure 1 shows the TEM bright-field image of as melt-spun ribbon. As seen from Fig. 1, the microstructure consists of fine eutectic phase and an α(Al) dendrite with dendrite arm spacing of about 0.472 μm. The cooling rate R can be calculated using the empirical relationship of $R=(45/\lambda)^{1/0.39}$ proposed by FLEMINGS et al [24] for an Al−4.5%Cu alloy, where λ is the dendrite arm spacing and R is the cooling rate. From the relation, the cooling rate is calculated to be 1.60×10^5 K/s. In the dendrite structure, Al_2CuMg precipitation phase prefers to precipitate along the dendritic boundaries, resulting in the formation of incontinuous stripe distribution. It suggests that the precipitation might have occurred during post-solidification cooling.

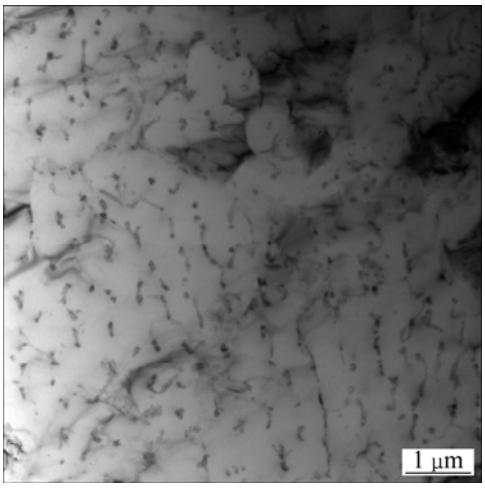

Fig. 1 TEM bright-field image of as melt-spun AlMgCu ribbon

Figures 2 and 3 show the micrographs, crystal structure and EDS results of constituent phases in T6 melt-spun AlMgCu ribbon. There are Al_2CuMg rhombohedral phase (see Figs. 2(a) and (b)) and amorphous SiO_2 (see Fig. 2(a), Figs. 3(a), (b) and (c)) in the microstructure of T6 melt-spun AlMgCu ribbon. The average chemical compositions of Al_2CuMg and SiO_2 constituent phases are listed in Table 2.

The most often observed phase is Al_2CuMg phase in AlMgCu alloy. For T6 melt-spun AlCuMg ribbon, it has a typical morphology of round-shaped, isolated particles with several dozens of nanometer in diameter, as shown in Figs. 2(a) and (b). The crystal structure of the particles

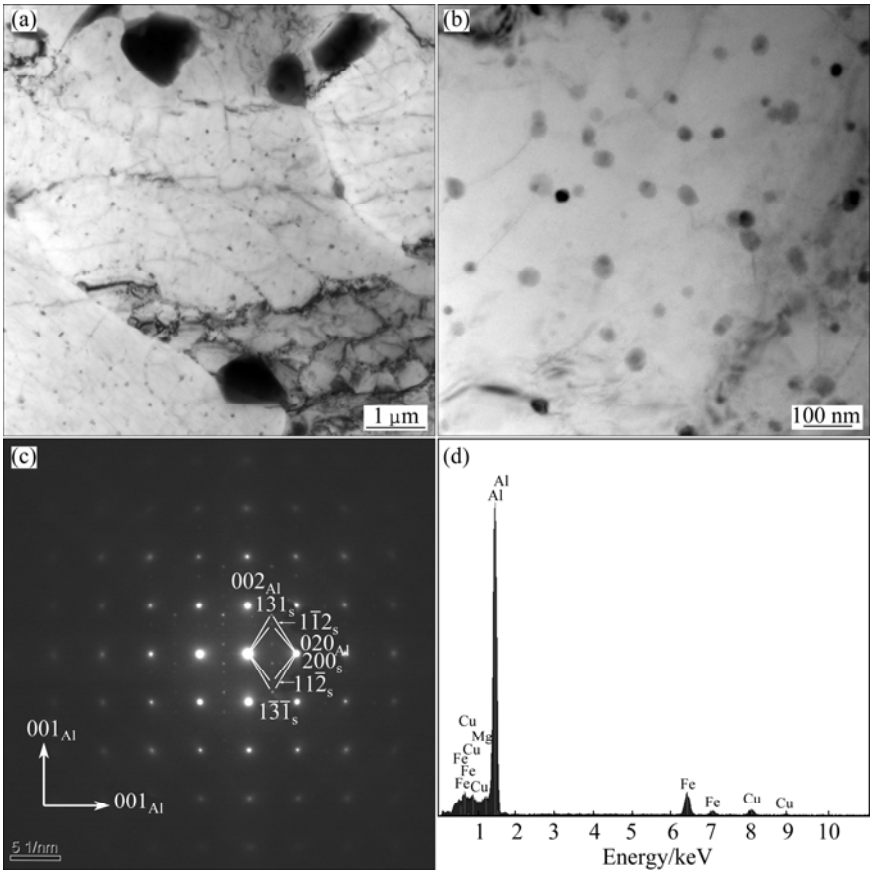

Fig. 2 TEM bright-field image (a, b), SAED pattern (c) viewed along $[100]_{Al}$ electron beam direction, and EDS spectrum (d) of Al_2CuMg phase in T6 melt-spun AlMgCu ribbon

Table 2 Average chemical composition of Al_2CuMg and SiO_2 constituent phases in T6 melt-spun AlMgCu ribbon

Sample	*x*(Al)/%	*x*(Mg)/%	*x*(Cu)/%	*x*(Fe)/%	*x*(Si)/%	*x*(O)/%
Al_2CuMg (this study)	88.80	2.97	2.88	5.35	−	−
Al_2CuMg [25]	51.60	23.52	24.00	0.08	−	−
SiO_2	2.07	−	−	−	31.61	66.31

is determined to be a face-centered orthorhombic structure by SAED pattern (Fig. 2(c)), which corresponds to the published works [13,19]. The measured composition shows the ratio of Cu and Mg is in good agreement with the stoichiometry of the Al_2CuMg phase, even though some amount of Fe is involved in the particles. In addition, higher Al concentration measured in the phase can result from confused Al in α(Al) matrix by EDS.

Amorphous SiO_2 particles are also found in the microstructure of T6 melt-spun AlMgCu ribbon, and these particles are proximately round-shaped and always appear to be dark in TEM bright-field images of Fig. 2(a), Figs. 3(a), (b) and (c). EDS results in Fig. 3(f) and Table 2 suggest that the concentration ratio of Si and O is close to 1:2 for these particles. Figures 3(d) and (e) show the HRTEM micrograph and SAED pattern of amorphous SiO_2, respectively. SAED pattern and HRTEM image of these particles show no evidence of crystallinity. Hence, it is determined that these particles are the amorphous SiO_2. Moreover, it presents that the amorphous SiO_2 particles preferentially precipitate along the grain boundaries from Figs. 3(b) and (c).

The microhardness values of the melt-spun AlMgCu ribbons and conventional DC samples are given in Table 3. In comparison with the conventional DC-T6 samples, the microhardness values of T6 melt-spun AlMgCu ribbon are increased by 28.5%, although there is no large change in microhardness value of two as-cast AlMgCu samples.

Table 3 Vickers microhardness values of melt-spun AlMgCu ribbons and conventional DC sample

Melt-spun		DC ingot	
As-melt-spun	T6	As- melt-spun	T6
69.8±2.8	130.7±3.6	67.2±1.5	101.7±6.7

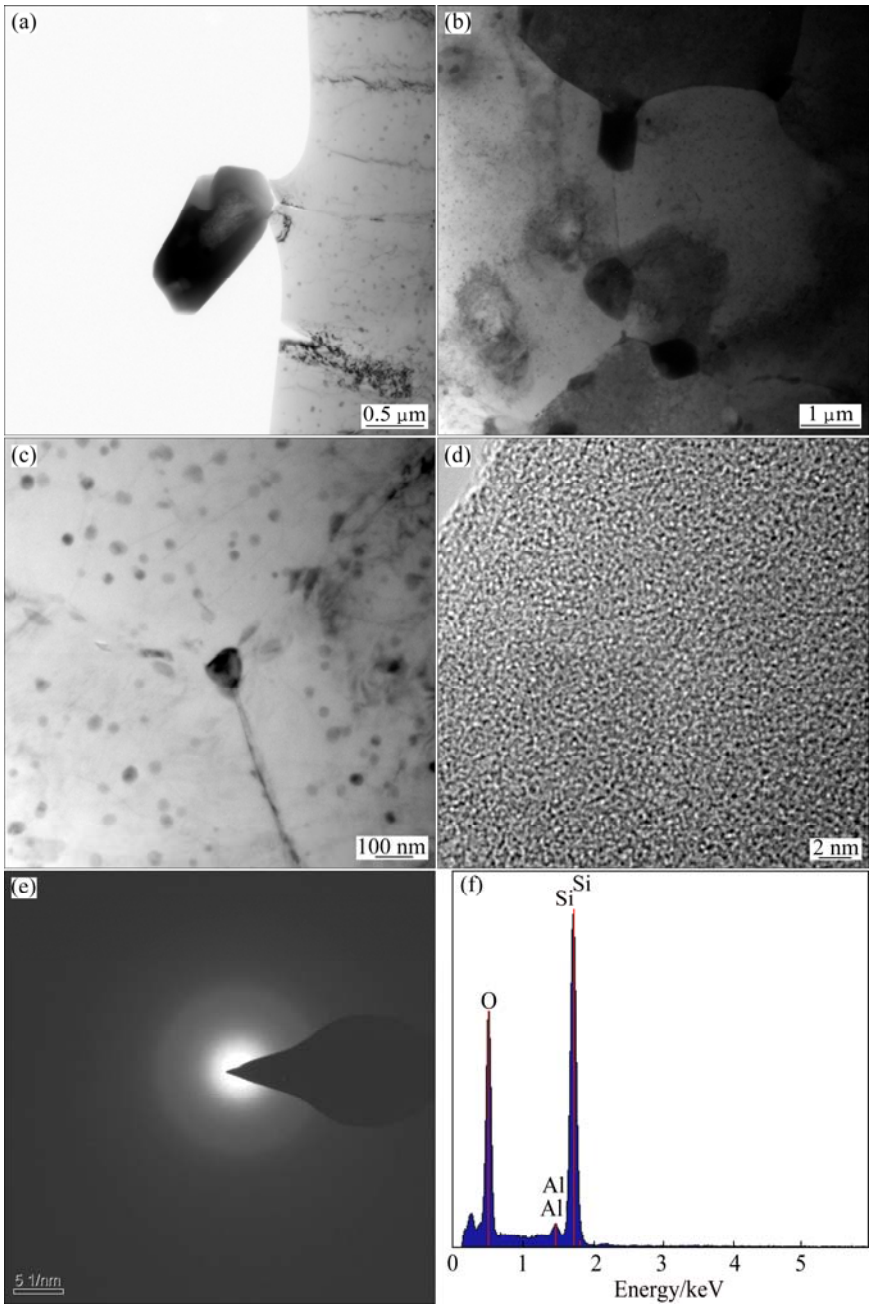

Fig. 3 TEM bright-field images (a,b,c), HRTEM micrograph (d), SAED pattern (e) and EDS spectrum (f) of amorphous SiO_2 in T6 melt-spun AlMgCu ribbon

4 Discussion

As discussed above, Al_2CuMg rhombohedral phase and abnormal amorphous SiO_2 are identified in the microstructure of T6 melt-spun AlMgCu ribbon by TEM technique with HRTEM, SAED and EDS. For the chemistry of the Al_2CuMg phases, the measured result is essentially in agreement with the published references [13,19]. Small deviation from their stoichiometric compositions, however, is observed from Table 2. These deviations reflect the influence of the alloy compositions on the phase chemistry and can be attributed to the substitution of elements in the compound by impurities and alloying elements. The results from this study suggest that transition element Fe could substitute for Al. This result indicates the nature of α(Al) matrix, which has an ability to dissolve limited amount of some elements, and may also reflect the complex influence of the industrial alloy system on the phase composition [25]. Moreover, the higher cooling rate during melt spinning can accommodate alloying element Fe in α(Al) matrix, and the Al_2CuMg phases with element Fe can easily precipitate. Nevertheless, the substitution of Al with small amount of transition elements can not change the

crystal structure of the phase.

The addition of trace amount of selected microalloying elements, such as Si and Ag, into age-hardening AlCuMg alloys can cause the changes in the nature of clustering and precipitation processes, which have a marked effect on mechanical properties. It was reported that the addition of Si into AlMgCu alloys with low Cu−Mg ratio can improve both the tensile and creep strengths [26]. WILSON et al [27] demonstrated that the room temperature age hardening response was delayed and the elevated temperature response was enhanced by Si addition. These effects were attributed to the extremely fine and uniformly dispersed GPB zones and a refined dispersion of *S* phase, which forms with a lath-shape elongated along $\langle 100\rangle_\alpha$ with a $\{210\}_\alpha$ habit planes. However, in this study, because of the rapid cooling rate during melt-spinning process, a significant proportion of the microalloying element Si can be dissolved into α(Al) matrix in melt-spun AlMgCu ribbon. Oxygen in the melt is prone to distributing along the dendritic boundaries during solidification. During artificial ageing, the long time and high temperature heat treatment promotes the elements diffusion. Therefore, the driving force for SiO_2 precipitation along the dendritic boundaries increases obviously and promotes SiO_2 precipitation by the surface oxide or residual oxygen during heat treatment.

Furthermore, according to previous researches [28,29], the formation of amorphous particles should be attributed to the interface stress between α(Al) and SiO_2. α(Al) and SiO_2 phases both have the cubic crystal structure, the crystal parameter of α(Al) is 0.4040 nm, while the crystal parameter of SiO_2 is 0.7166 nm [30]. Therefore, it is no doubt that the difference in crystal parameter would result in great stress along phase interface. Based on the recent research [31], the high interface stress can result in the formation of abnormal amorphous SiO_2 particles. Moreover, the Gibbs free energies of the amorphous SiO_2 and Mg_2Si compound at 298 K are −850.70 kJ/mol and −99.51 kJ/mol, respectively [32]. Subsequently, for T6 melt-spun AlMgCu ribbon, it is preferential to form the SiO_2 particles, rather than the compound Mg_2Si, which is different from the result in Ref. [7].

In order to correlate the structural features with the mechanical behavior of the melt-spun AlMgCu ribbons, Vickers microhardness test was performed, and the results are listed in Table 3. From Refs. [7,15,33], the microhardness value of the alloy ribbon aged at 200 °C for 16 h in this study is quite close to the peak hardness, which can be attributed to the fine dispersion of the Al_2CuMg phase. However, the formation of amorphous SiO_2 precipitation has no significant effect on the microhardness. High microhardness value of T6 melt-spun AlMgCu ribbon could be derived from the rapid cooling rate in melt-spinning process and the recrystallization after ageing.

5 Conclusions

1) The cooling rate of as melt-spun AlMgCu ribbon is estimated to be 1.60×10^5 K/s from the empirical relationship.

2) Al_2CuMg and abnormal amorphous SiO_2 constituent phases are identified in T6 melt-spun AlMgCu ribbon.

3) The formation of abnormal amorphous SiO_2 appears to be associated with the higher cooling rate in melt-spinning process and has no significant effect on the peak hardness.

References

[1] KOVARIK L, MILLER M K, COURT S A, MILLS M J. Origin of the modified orientation relationship for *S*(*S*″)-phase in Al−Mg−Cu alloys [J]. Acta Materialia, 2006, 54(7): 1731−1740.

[2] WINKELMAN G B, RAVIPRASAD K, MUDDLE B C. Orientation relationships and lattice matching for the *S* phase in Al−Cu−Mg alloys [J]. Acta Materialia, 2007, 55(9): 3213−3228.

[3] KOVARIK L, COURT S A, FRASER H L, MILLS M J. GPB zones and composite GPB/GPBII zones in Al−Cu−Mg alloys [J]. Acta Materialia, 2008, 56(17): 4804−4815.

[4] KOVARIK L, GOUMA P I, KISIELOWSKI C, COURT S A, MILLS M J. A HRTEM study of metastable phase formation in Al−Mg−Cu alloys during artificial aging [J]. Acta Materialia, 2004, 52(9): 2509−2520.

[5] FENG Z Q, YANG Y Q, HUANG B, HAN M, LUO X, RU J G. Precipitation process along dislocations in Al−Cu−Mg alloy during artificial aging [J]. Materials Science and Engineering A, 2010, 528(2): 706−714.

[6] WANG S C, STARINK M J, GAO N. Precipitation hardening in Al−Cu−Mg alloys revisited [J]. Scripta Materialia, 2006, 54(2): 287−291.

[7] HUTCHINSON C R, RINGER S P. Precipitation processes in Al−Cu−Mg alloys microalloyed with Si [J]. Metallurgical and Materials Transactions A, 2000, 31(11): 2721−2733.

[8] RAVIPRASAD K, HUTCHINSON C R, SAKURAI T, RINGER S P. Precipitation processes in an Al−2.5Cu−1.5Mg (wt. %) alloy microalloyed with Ag and Si [J]. Acta Materialia, 2003, 51(17): 5037−5050.

[9] RINGER S P, SOFYAN B T, PRASAD K S, QUAN G C. Precipitation reactions in Al−4.0Cu−0.3Mg (wt.%) alloy [J]. Acta Materialia, 2008, 56(9): 2147−2160.

[10] RATCHEV P, VERLINDEN B, de SMET P, van HOUTTE P. Precipitation hardening of an Al−4.2 wt% Mg−0.6 wt% Cu alloy [J]. Acta Materialia, 1998, 46(10): 3523−3533.

[11] BAGARYATSKY Y A. Structural changes on aging Al−Cu−Mg alloys [J]. Dokl Akad SSSR, 1952, 87: 397−559.

[12] SILCOCK J M. The structural ageing characteristics of Al−Cu−Mg alloys with copper: magnesium weight ratios of 7:1 and 2.2:1 [J]. Journal of the Japan Institute of Metals, 1960−1961, 89: 203−210.

[13] WANG S C, STARINK M J. Precipitates and intermetallic phases in

precipitation hardening Al−Cu−Mg−(Li) based alloys [J]. International Materials Reviews, 2005, 50: 193−215.
[14] RADMILOVIC V, KILLAS R, DAHNEN U, SHIFLET G J. Structure and morphology of *S*-phase precipitates in aluminum [J]. Acta Materialia, 1999, 47(15−16): 3987−3997.
[15] RINGER S P, POLMEARB I J, SAKURAI T. Effect of additions of Si and Ag to ternary Al−Cu−Mg alloys in the α+*S* phase field [J]. Materials Science and Engineering A, 1996, 217−218: 273−276.
[16] VIETZ J T, POLMEAR I J. The influence of small additions of silver on the aging of aluminum alloys [J]. Jouranl of the Japan Institute of Metals, 1966, 94: 410−421.
[17] GABLE B M, SHIFLET G J, STARKE E A Jr. The effect of Si additions on Ω precipitation in Al−Cu−Mg-(Ag) alloys [J]. Scripta Materialia, 2004, 50(1): 149−153.
[18] MUKHOPADHYAY A K. Coprecipitation of Ω and σ phases in Al−Cu−Mg−Mn alloys containing Ag and Si [J]. Metallurgical and Materials Transactions A, 2002, 33(12): 3635−3648.
[19] WANG S C, STARINK M J. Two types of *S* phase precipitates in Al−Cu−Mg alloys [J]. Acta Materialia, 2007, 55(3): 933−941.
[20] BIROL Y. Microstructural evolution during annealing of a rapidly solidified Al−12Si alloy [J]. Journal of Alloys and Compounds, 2007, 439(1−2): 81−86.
[21] SHALABY R M. Effect of rapid solidification on mechanical properties of a lead free Sn−3.5Ag solder [J]. Journal of Alloys and Compounds, 2010, 505(1): 113−117.
[22] KALAY Y E, CHUMBLEY L S, ANDERSON I E, NAPOLITANO R E. Characterization of hypereutectic Al−Si powders solidified under far-from equilibrium conditions [J]. Metallurgical and Materials Transactions A, 2007, 38(7): 1452−1457.
[23] LÓPEZ I A, ZEPEDA C M, REYES J G G, FLORES A M, RODRÍGUEZ J S, GÓMEZ L B. TEM microstructural characterization of melt-spun aged Al−6Si−3Cu−*x*Mg alloys [J]. Materials Characterization, 2007, 58(6): 509−518.
[24] FLEMINGS M C, KATTAMIS T Z, BARDES B P. Dendrite arm spacing in aluminum alloys [J]. AFS Transactions, 1991, 99: 501−506.
[25] GAO M, FENG C R, WEI R P. An analytical electron microscopy study of constituent particles in commercial 7075-T6 and 2024-T3 alloys [J]. Metallurgical and Materials Transactions A, 1998, 29(4): 1145−1151.
[26] POLMEAR I J. Light alloys: Metallurgy of the light metals [M]. 3rd ed. London: Arnold, 1995.
[27] WILSON R N, MOORE D M, FORSYTH P J E. Effects of 0.25% silicon on precipitation processes in an aluminum−0.25% copper−1.2% magnesium alloy [J]. Jouranl of the Japan Institute of Metals, 1967, 97: 177−182.
[28] SHENG L Y, YANG F, XI T F, LAI C, YE H Q. Influence of heat treatment on interface of Cu/Al bimetal composite fabricated by cold rolling [J]. Composites Part B: Engineering, 2011, 42(6): 1468−1473.
[29] AMINI R, SHOKROLLAHI H, SALAHINEJAD E, HADIANFARD M J, MARASI M, SRITHARAN T. Microstructural, thermal and magnetic properties of amorphous/nanocrystalline FeCrMnN alloys prepared by mechanical alloying and subsequent heat treatment [J]. Journal of Alloys and Compounds, 2009, 480(2): 617−624.
[30] PEACOR D R. High-temperature single-crystal study of the cristobalite inversion [J]. Zeitschrift für Kristallographie, Kristallgeometrie, Kristallphysik, Kristallchemie, 1973, 138: 274−298.
[31] SHENG L Y, YANG F, GUO J T, XI T F, YE H Q. Investigation on NiAl–TiC–Al_2O_3 composite prepared by self-propagation high temperature synthesis with hot extrusion [J]. Composites Part B: Engineering, 2013, 45: 785−791.
[32] KUBASCHEWSKI O, ALCOCK C B. Metallurgical thermochemistry [M]. 5th ed. Oxford: Pergamon Press, 1967.
[33] RAVIPRASAD K, MOUTSOS S. Early stage hardening in Al−Cu−Mg alloys [J]. Materials Forum, 2004, 28: 412−417.

T6 态 AlMgCu 铝合金激冷甩带的反常析出行为

陈忠伟，汤明军，李士顺，冯宗强

西北工业大学 凝固技术国家重点实验室，西安 710072

摘　要：利用高分辨透射电镜和硬度测试表征时效态 AlMgCu 铝合金激冷甩带的析出相组成。铸态合金甩带的冷却速率通过经验公式计算为 1.60×10^5 K/s。T6 态热处理是试样经固溶处理后再进行 200 °C 保温 16 h 的时效处理。结果表明，T6 态 AlMgCu 铝合金激冷甩带含有 Al_2CuMg 相和反常非晶 SiO_2 两种析出相。Al_2CuMg 析出相的晶体结构和成分配比与文献[Wang et al.(2007; 2005)]结果一致。综合实验结果分析表明，反常非晶 SiO_2 相的析出可能与激冷甩带具有高的冷却速率有关，它的析出对其硬度的影响不大。

关键词：AlCuMg 合金；熔体激冷；析出；非晶

(Edited by Hua YANG)